Article

Investigation and Statistical Analysis for Optimizing Surface Roughness, Cutting Forces, Temperature, and Productivity in Turning Grey Cast Iron

Magdy M. El Rayes [1,*], **Adel T. Abbas** [1], **Abdulhamid A. Al-Abduljabbar** [1], **Adham E. Ragab** [2], **Faycal Benyahia** [1] **and Ahmed Elkaseer** [3]

[1] Department of Mechanical Engineering, College of Engineering, King Saud University, P.O. Box 800, Riyadh 11421, Saudi Arabia; aabbas@ksu.edu.sa (A.T.A.); ajabbar@ksu.edu.sa (A.A.A.-A.); fbenyahia@ksu.edu.sa (F.B.)

[2] Department of Industrial Engineering, College of Engineering, King Saud University, P.O. Box 800, Riyadh 11421, Saudi Arabia; aragab@ksu.edu.sa

[3] Institute for Automation and Applied Informatics, Karlsruhe Institute of Technology, 76344 Eggenstein-Leopoldshafen, Germany; ahmed.elkaseer@kit.edu

* Correspondence: melrayes@ksu.edu.sa

Abstract: This paper investigated the influence of cutting parameters, including feed rate, cutting speed, tool nose radius, and wet or dry cutting conditions, on the resultant force, cutting edge/workpiece temperature, and surface roughness when turning grey cast iron. Results showed that increasing the feed rate increased the resultant force, cutting temperature, and surface roughness. At the same time, increasing the cutting speed and nose radius increased the cutting temperature, which in turn reduced the resultant force. For practical applications, basic mathematical calculations based on the sole effect of each parameter on the output of the experiments were used to estimate the extent of percentage increase in cutting temperature due to increasing feed rate, cutting speed, and nose radius. Similarly, the same approach was used to estimate the effect of increasing feed rate, cutting speed, and nose radius on average surface roughness. Results showed that increasing the feed rate increases the cutting temperature by 5 to 11% depending on the nose radius and cutting speed. On the other hand, increasing the cutting speed was found to have limited effect on cutting temperature with small nose radius whereas this effect increases with increasing the nose radius reaching about 11%. Increasing the nose radius also increases the cutting temperature, depending mainly on cutting speed, reaching a maximum of 21% at higher cutting speeds. Results also showed that increasing the feed rate increased the average surface roughness considerably to about 120% at high cutting speeds and a large nose radius. On the other hand, increasing the cutting speed and nose radius reduced the surface roughness (i.e., improved surface quality) by a maximum of 29 and 23%, respectively. In order to study the combined effects of the cutting parameters on the three responses, namely, the resultant cutting force, cutting temperature, and surface roughness, full factorial design and ANOVA were used, where it was found to be in good agreement with mathematical calculations. Additionally, the desirability function optimization tool was used to minimize the measured responses whilst maximizing the material removal rate.

Keywords: resultant cutting force; cutting temperature; cutting parameters; grey cast iron; optimization; surface roughness

1. Introduction

Grey cast iron has a graphitic microstructure where its mechanical properties are controlled by the size and shape of the graphite flakes and also has a high ability to dampen vibrations. This makes this type of cast iron an ideal selection for machinery bases, housing applications, cylinder blocks, and internal combustion engines. Undoubtedly, such

applications require numerous machining processes; therefore, the machinability of grey cast iron is considered as prime concern in this field of research. Chen et al. [1] studied the machinability of cast iron, comparing cemented carbide tool (WTVC8) composed of W, Ti, V, Co with plain (WC8) composed of W and Co when cutting HT250 grey cast iron in a machining test. The former tool had longer tool life due to higher hot hardness. It was also reported that the dominant flank wear mechanism was adhesion wear and oxidation. The tool life model, serving as a guide for optimization of cutting performance, showed that the cutting speed "V_c" is the most influential parameter on tool life and, to a lesser extent, the depth of cut "DOC" and feed rate "FR". Fischer et al. [2] conducted turning experiments on grey cast iron using WC insert and established a multi-objective goal optimization model suggesting that the "V_c" and "FR" can be calculated and altered aiming to a specific surface roughness. Cutting tool performance was evaluated by Souza et al. [3], who conducted turning runs on grey cast iron using a Si_3N_4-based ceramic tool at various "V_c" and "FR", whereas the "DOC" was maintained constant. The cutting forces, cutting temperature, flank wear, and surface roughness were measured to evaluate tool performance. The Si_3N_4 ceramic tool showed a high performance even at higher "V_c" due to its high hot hardness and the presence of graphite flakes which lower the friction coefficient between the tool and workpiece, thus reducing the cutting temperature. Increasing the "V_c" increased the cutting forces to 300 m/min, beyond which cutting forces decreased due to thermal degradation. Furthermore, higher feed rates increased the cutting force components, whereas it slightly reduced the average cutting temperature after it was initially increased. Meng et al. [4] applied a novel method in simulation to establish a microstructural model while investigating the machinability of graphite iron. The chip and cut surface morphologies, their formation mechanisms, and cutting temperature distribution were studied through the application of MATLAB image recognition and Python programming. The simulation showed that during cutting, cracks develop on the chip surface, and graphite particles occur, leaving cavities on the cut surface. The reason for this result was the stress concentration at the graphite/pearlite matrix interface. Rajbongshi et al. [5] optimized the "V_c", feed, and DOC by applying Taguchi's Orthogonal Array and Analysis of Variance (ANOVA) when turning grey cast iron using a mixed oxide ceramic tool in dry and air-cooled conditions. The main cutting and feed forces, flank wear, and surface roughness have the greatest effect when determining the optimum turning parameters. In dry turning, the feed is the most affecting parameter on surface roughness and cutting force, whereas, in air-cool turning, the "V_c" and DOC, as well as feed interaction, are the most affecting variables on flank wear. In addition, it was concluded that air-cooled turning is a better selection compared to the dry one with respect to the flank wear, cutting, and feed forces, whereas dry turning is favored over air-cooled turning in changing surface roughness. Korkmaz and Günay [6] investigated the effects of machining parameters on cutting forces and power consumption while turning AISI 420 martensitic stainless steel with coated cemented carbide tools by using the finite element method where its validation model was approved when compared with experimental cutting forces and power consumption. In addition, the analysis of variance (ANOVA) showed that cutting speed has a significant effect on power consumption. Asiltürk et al. [7] measured the surface roughness, vibration, and acoustic emission values, which were measured after turning experiments of AISI 4140 steel on a CNC machine. A rule-based fuzzy logic model was created using MATLAB program, after which the fuzzy model results were compared with experimental ones, which showed that the rule-based fuzzy logic model is quite successful. The influence of different machining parameters on the cutting tip temperature and surface roughness of as-received and annealed cast iron was studied by Ogedengbe et al. [8]. Taguchi's design from Minitab 18 was applied to determine the optimum cutting parameters and analysis of the effect of these parameters on tool-tip temperature, which was reduced when increasing the spindle speed and, to a lesser extent, the feed rate and then DOC. It was concluded that annealing cast iron improves surface finish, especially when using cutting fluid, compared to dry cuts. The effect of milling

cutting parameters and lubrication on the machinability characteristics of mold steel was studied and analyzed by Binali et al. [9]. Milling cutting runs were conducted according to full factorial design, altering the parameters of cutting speed, feed rate, depth of cut, and lubrication. It was reported that irrespective of the cutting conditions, the main wear type was nose wear occurring at the tool edge, and its magnitude varied when cutting speed and lubrication type were changed. It was also reported that the cutting speed and the feed rate most significantly affected the cutting temperature. Abbas et al. [10] experimentally and statistically investigated, the effect of conventional and wiper tool edge geometries on the surface roughness, the cutting forces, the cutting temperature, and the material removal rate. They compared the machining performance obtained using wiper inserts with those obtained using conventional round-nose inserts. The results reveal that the optimum material removal rate for wiper-shaped inserts is 67% greater than that of conventional inserts while maintaining a 0.7 µm surface roughness value. The superior results obtained with wiper-shaped inserts allow wiper tools to use higher feed rates, resulting in larger material removal rates while obtaining the same surface quality. Abbas et al. [11,12] used Taguchi's robust design to optimize surface roughness, considering the tool nose radius and coolant as noise factors. They developed a predictive model to determine the optimum combination of control factors for different configurations of noise factors. The results show low prediction errors (5%) when compared to real experimental tests. An optimum combination of 150 m/min surface speed, 0.64 mm depth of cut, and 0.05 mm/rev feed rate is used in case of an uncertain combination of tool nose radius and coolant condition. Turning of AISI 5140 steel was conducted by Kuntoğlu and Sağlam [13], where on-line measurements of the temperature of the cutting tool tip, acoustic emission, and off-line measurement of the cutting tool flank wear (for tool life evaluation) were performed. It was found that the combined effect of depth of cut and cutting-edge angle had an effect (40%) on flank wear, whereas the cutting speed and cutting-edge angle had a dominant effect on temperature (45.4%) and AE (46.23%), respectively. The objective of the present work is to study the influence of the machining parameters, namely, "V_c", feed rate, tool nose radius, and the presence or absence of cutting fluid on the process outputs, which is resultant force, cutting temperature, and surface roughness. In addition, another objective is to study and optimize the effects of these parameters on the same process outputs using full factorial design and ANOVA.

2. Materials and Methods

The material used in this work was as-cast SAE J431- grey cast iron, SAE grade G1800. Tables 1 and 2 present the chemical composition and the mechanical properties of grey cast iron, respectively. The material's thermal conductivity is 43 W/m-K, specific heat capacity is 490 J/kg-K, and thermal expansion is 13 µm/m-K.

Table 1. Chemical composition of grey cast iron.

Element	C	Fe	Mn	Si	P	S
wt. %	3.6	93	0.65	2.3	0.15	0.14

Table 2. Mechanical properties of grey cast iron.

Properties	Value
Ultimate tensile strength, MPa	140
Yield strength (Proof), MPa	94
Elongation at break, %	14
Modulus of elasticity (Typical for steel), GPa	180
Hardness, HV10	185

The microstructure of the grey cast iron used is shown in Figure 1a,b in the unetched and etched conditions, respectively, which is typically pearlitic-grey iron. The graphite flakes are interconnected in the form of network where their tips are somewhat sharp, as shown in Figure 1a, whereas the fully pearlitic microstructure and few graphite flakes can be seen at higher magnification, as shown in Figure 1b.
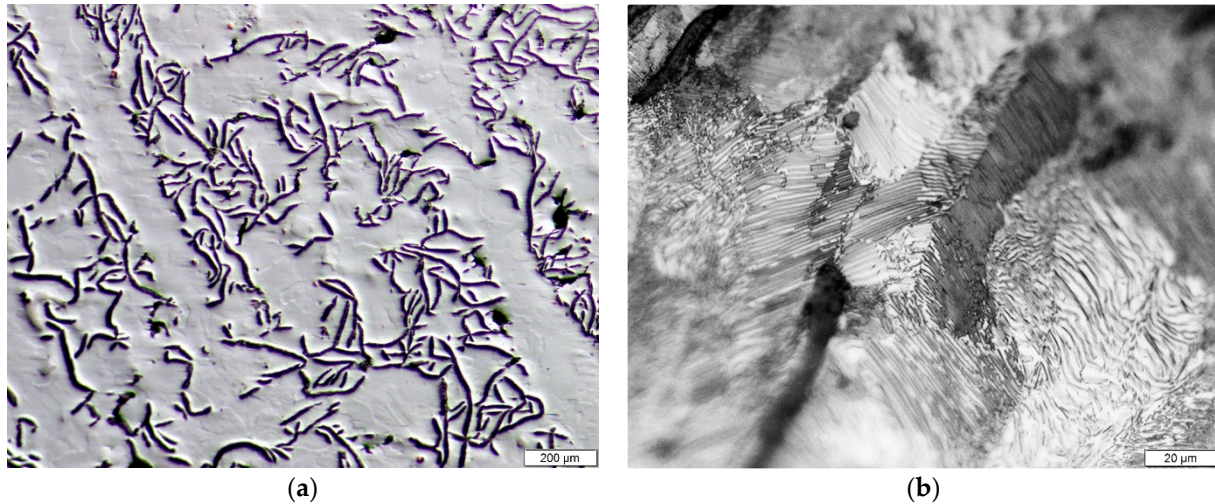

| (**a**) | (**b**) |

Figure 1. Optical microscope images of the microstructure of as-received grey cast iron: (**a**) unetched, low magnification; (**b**) etched, high magnification.

A conventional turning machine (type EMCOMAT- 20D by Emco Company (Salzburg, Austria)) was used for machining the test pieces. It has 5.3 kw drive motor, with electronic speed controls up to 3000 rpm. Three longitudinal feed rates were within the experiments 0.056, 0.112, and 0.168 mm/rev. The turning tool selected is commonly used for machining grey iron and was manufactured by Sandvik (Stockholm, Sweden). A tool holder (type DCLNR2020K12) and three inserts with different nose radii of 0.4, 0.8, and 1.2 mm, with commercial codes CNMG120404-KF3225, CNMG120408-KF3225, and CNMG120412-KF3225, respectively, were used to conduct machining runs. The workpiece was 250 mm long, 60 mm in diameter, and the total length for cut was divided into three equal zones of 15 mm, each of which was separated by a recess and was cut using a specific feed rate. The tool holder was mounted on a 3-component piezoelectric force dynamometer (Kistler 5070) equipped with software "Dynoware" type 2825A (Liechtenstein, Switzerland), which was used for measuring the three cutting force components, namely, radial force (F_r), feed force (F_f), and main cutting force (F_c). As already known, cutting forces arising during turning consist of the main cutting (F_c), feed (F_f), and radial (F_r) force components, all of which, when combined, yield to the resultant force (R), as in Equation (1). The direction/line of action of these force components F_c, F_f, and F_r is tangential, axial, and radial directions, respectively.

$$R = \sqrt{F_r^2 + F_f^2 + F_c^2} \tag{1}$$

All forces were measured in Newton (N). The material removal rate (MRR) was calculated from Equation (2):

$$MRR = 1000V_c \times FR.DOC \tag{2}$$

where V_c = Surface speed (m/min), FR = Feed rate (mm/rev.), DOC = depth of cut (mm) and MRR in (mm^3/min). In order to measure the temperature arising while cutting, a thermographic camera of the type ThermoPro-TP8, provided by Guide (Wuhan, China), was used to capture thermal images while cutting. The specifications of this camera are presented in Table 3:

Table 3. The specifications of thermographic camera.

Thermal Sensitivity:	$\leq$0.08 °C at 30 °C
Measuring range:	-20–1000 °C
Detector type:	Micro-bolometer-UFPA384 $\times$ 288 pixels
Spectral Range:	8–14 µm
Accuracy:	± 2 °C

The camera was calibrated manually to ascertain suitable focusing to the zone of interest where the temperature was measured, which is the interface between the cutting edge and the workpiece. The test rig for machining experiments is shown in Figure 2. A surface tester type "Rugosurf 90-G" from Tesa (Bugnon, Switzerland) was used to measure the surface roughness *Ra*, which was repeated five times to obtain average surface roughness Ra_{avg}. The measurement settings were cut-off length = 0.8 mm, measurement surface: curved, and measuring speed = 1 mm/s.
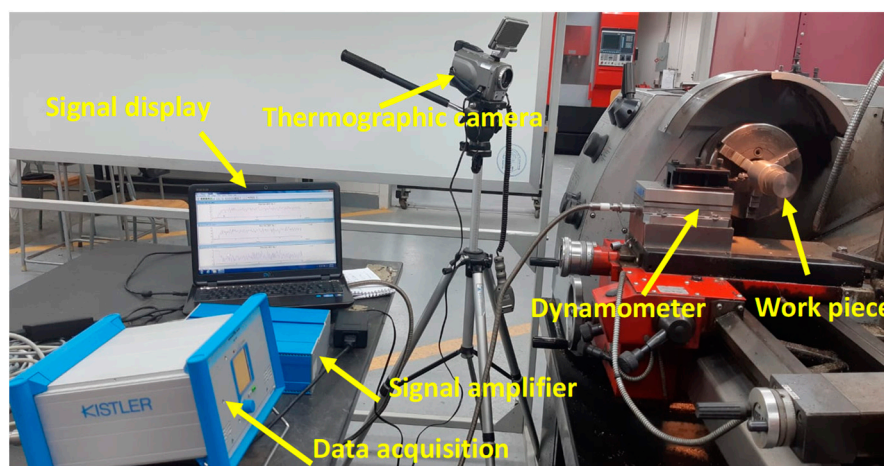
Figure 2. Test rig for machining the test pieces, measuring cutting forces and temperature.

Full factorial design, with four factors, was used to build the experiments matrix. The experimental plan was set with 36 test runs as follows: two levels of "V_c", three levels of feed rate, three levels of nose radius, and two levels of coolant. Table 4 summarizes the factors and their levels. The full matrix is illustrated in the next section with the measured responses. Minitab 18 was used to check the significance of the four factors, and their interactions, with the responses through ANOVA. Backward elimination was applied to remove the non-significant items from ANOVA one at a time.

Table 4. The experimental machining parameters and their levels.

Designation	Process Parameter	Level 1	Level 2	Level 3
V_c	Cutting Speed (m/min)	80	120	-
FR	Feed Rate (mm/rev.)	0.056	0.112	0.168
r	Nose Radius (mm)	0.4	0.8	1.2
Coolant	Coolant	On	Off	-

3. Results and Discussion

3.1. Effect of Feed Rate, Cutting Speed, and Nose Radius on the Resultant Force

Figure 3a,b show the effect of increasing the feed rate "*FR*" on the resultant force "*R*" in the dry and wet conditions, respectively. Increasing "*FR*" (mm/rev) increases "*R*"

due to the increase in the volume of workpiece material ahead of the cutting edge that is sheared/removed per revolution, which can generate higher compressive forces, thus leading to higher "R" Aouici et al. [14], and Chen et al. [15]. The same figure also shows that the "R" magnitude corresponding to V_c = 80 m/min is always higher than that with 120 m/min with all tool nose radii Chen et al. [15], and Thakur et al. [16]. The reason for this trend is probably due to the higher temperature/heating occurring with higher speed than that with lower speed. The higher temperature at the shear plane region leads to softening of the primary deformation zone, i.e., the shear zone, hence reducing its shear strength and consequently lowering the "R" required for cutting. Cutting fluid generally reduces all "R" values compared to the dry conditions and also its absolute difference at different "V_c" and nose radii, as shown in Figure 3b.
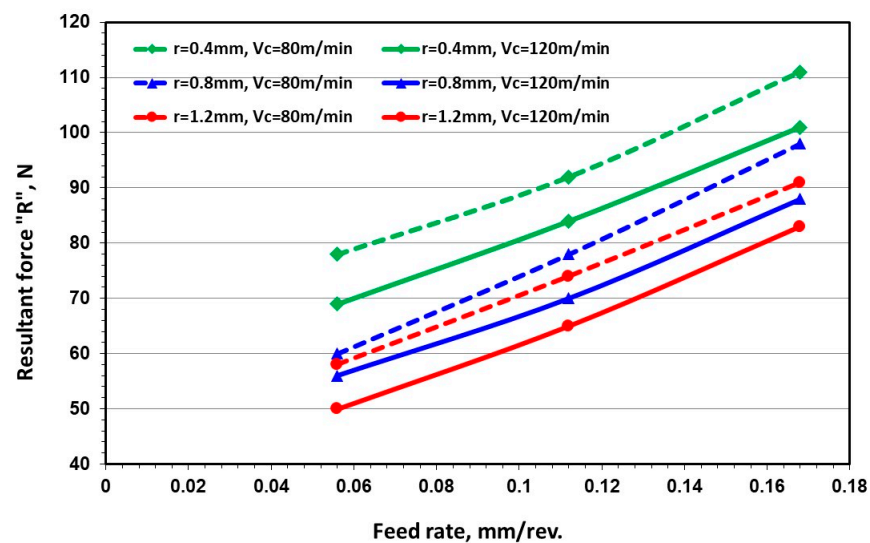
(**a**)
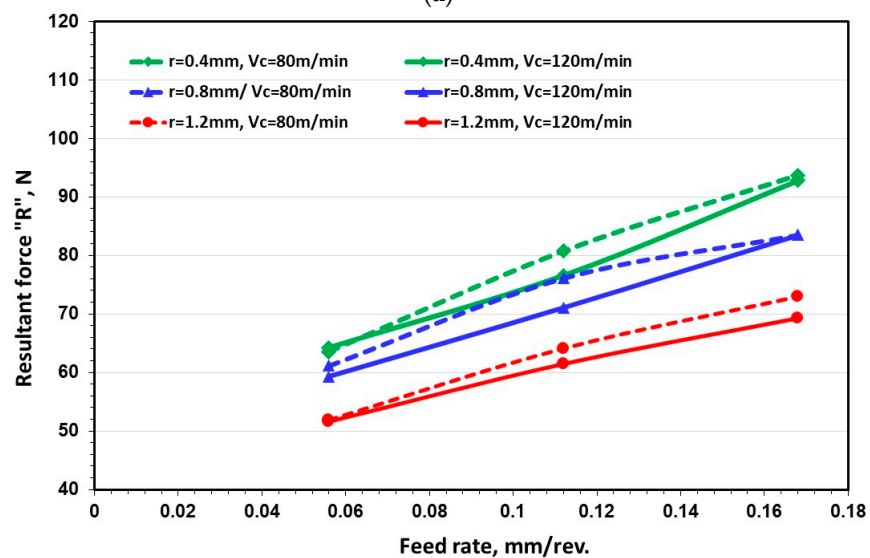
(**b**)

Figure 3. The relation between feed rate and resultant force at different cutting speeds and tool nose radii in (**a**) dry condition and (**b**) wet condition.

The effect of increasing "r" on "R" can also be deduced from Figure 3a,b, where it can be seen that a bigger "r" results in the reduction of "R" as reported by Ali and Ansari [17]. This may also be due to the cutting temperature "T", where a bigger "r" leads to a larger area of contact between the cutting edge and work material which consequently leads

to higher friction and, thus, a higher temperature within the cutting zone as found by Bouchelaghem et al. [18]. To better visualize the effect of "*r*" on the "*R*" in dry cutting, Figure 4a,b show this effect at "*V_c*" 80 and 120 m/min, respectively. With both "*V_c*", increasing "*r*" at constant "*FR*" is accompanied by a reduction in "*R*" due to higher heating, as mentioned earlier. In addition, the "*R*" values corresponding to each "*r*" is lower with V_c = 120 m/min than with 80 m/min. Thus, it can be stated that in dry cutting, the use of higher "*V_c*" yields lower "*R*".
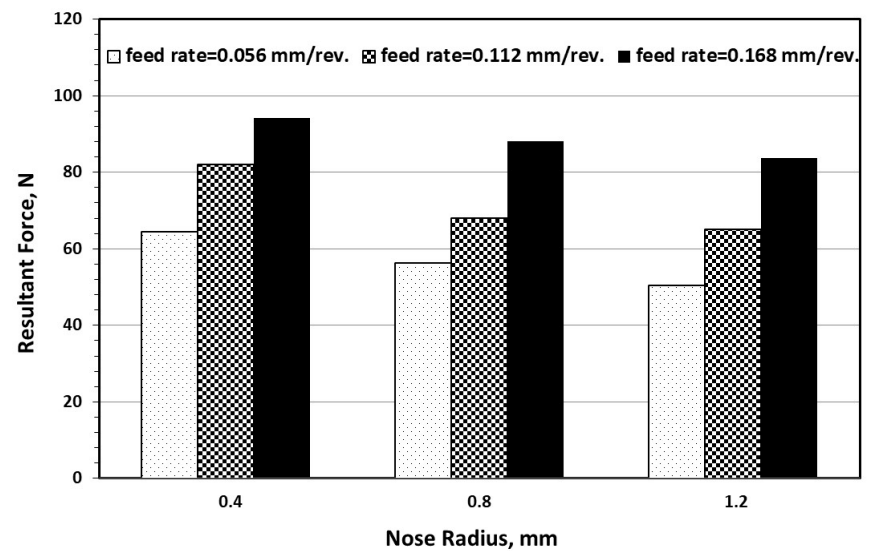
(**a**)
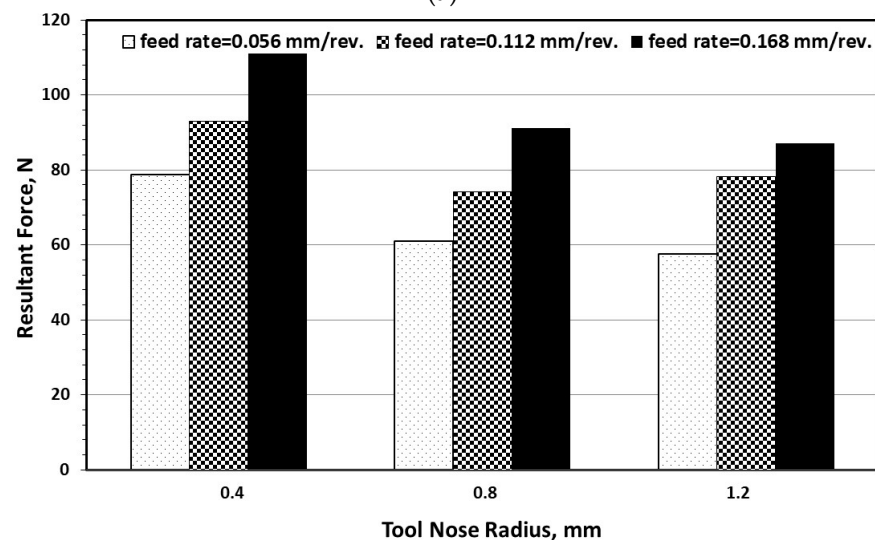
(**b**)

Figure 4. The effect of increasing tool nose radius on the resultant force at different cutting speeds: (**a**) 80 m/min and (**b**) 120 m/min.

To justify that a larger "*r*" leads to a longer length of contact between the tool and workpiece, the software SolidWorks was used to schematically show the overall contact length corresponding to nose radii used in this work. Figure 5a shows the general configuration of the tool and workpiece. Figure 5b–d show the overall contact length calculated by SolidWorks software, giving the values of 0.8139, 0.9752, and 1.1365 mm corresponding to "*r*" of 0.4, 0.8, and 1.2 mm, respectively. Figure 5e–g show stereomicroscope images of the actual inserts. Since the "*T*" measured at the cutting edge/workpiece interface evolves due

to increasing "*FR*", "*V_c*", and "*r*", it is, therefore, necessary to evaluate the contribution of each of these parameters in raising the "*T*".
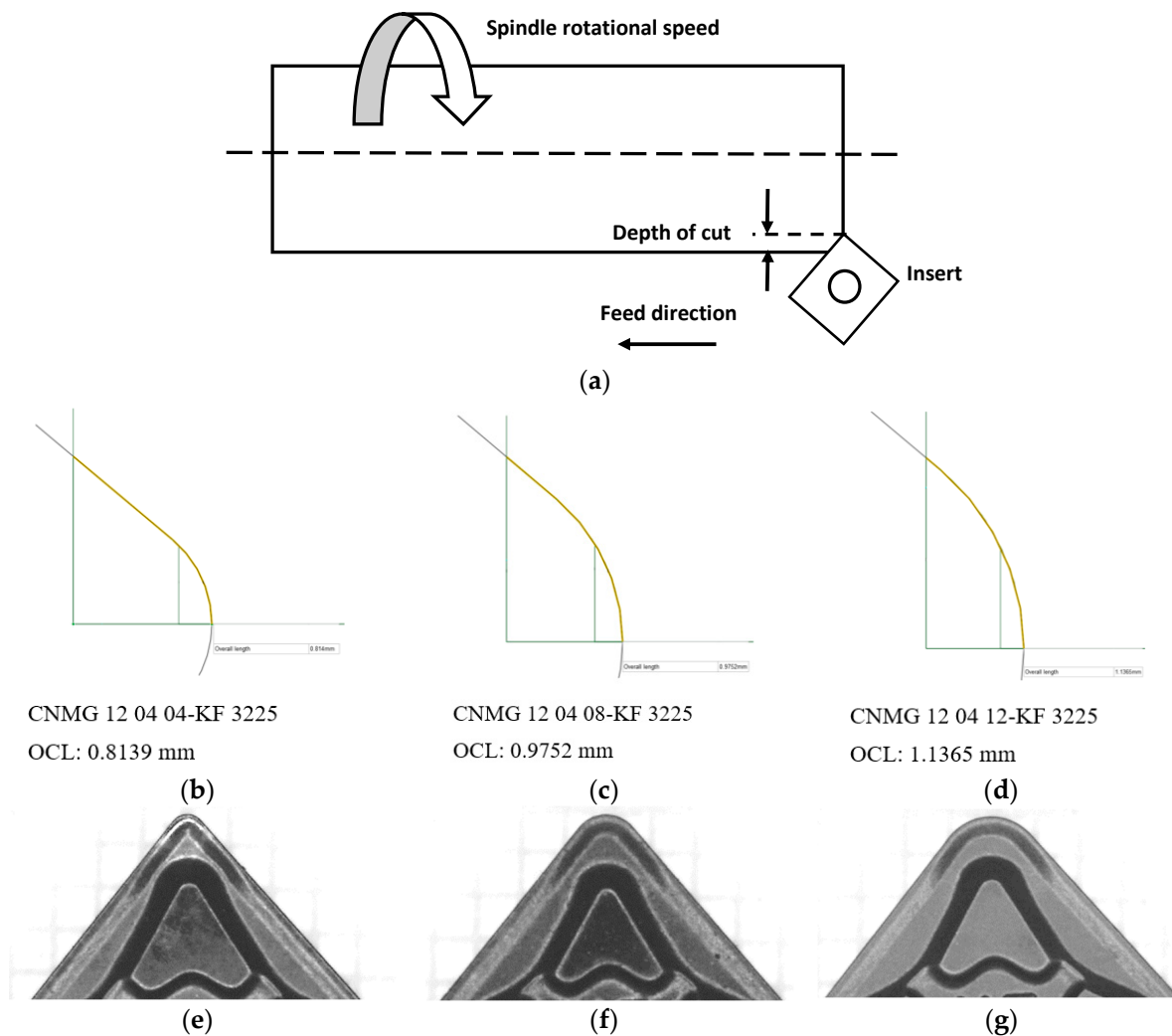

Figure 5. Simulation of the insert tool nose radius with the workpiece: (**a**) general configuration; overall contact length (OCL) measured using SolidWorks at (**b**) 0.4 mm, (**c**) 0.8 mm, and (**d**) 1.2 mm; stereomicroscope images ×5 of cutting inserts at (**e**) 0.4 mm, (**f**) 0.8 mm, and (**g**) 1.2 mm.

3.2. Effect of Feed Rate, Cutting Speed, and Nose Radius on Cutting Temperature

Figure 6 shows the relation between "*FR*" and the "*T*", which is almost linear as reported by Aouici et al. [14] and Bouchelaghem [18]. The same figure indicates that at constant "*FR*", higher "*V_c*"; i.e., a speed of 120 m/min is always accompanied by a higher temperature at all nose radii compared to that of 80 m/min. It is also observed that the highest "*T*" occurs with the biggest "*r*" and is gradually reduced when decreasing it. These results are in good agreement with the analysis mentioned earlier related to the "*R*". Comparing Figure 6a,b shows the logical influence of using cutting fluid during machining, wherein dry cutting resulted in "*T*" of around 350 °C, whereas wet cutting resulted in 156 °C.

Table 5 presents the effect of increasing "*FR*" at fixed "*V_c*" = 80 m/min on the average percentage increase in temperature ($T_{avg.}$ %), which was 4.6% with ($r = 0.4$ mm), 10.4% ($r = 0.8$ mm), and 10.3% ($r = 1.2$ mm), whereas, at "*V_c* = 120 m/min", the $T_{avg.}$ % was 5.0, 11.1, and 4.8%, with $r = 0.4$, 0.8, and 1.2 mm, respectively.
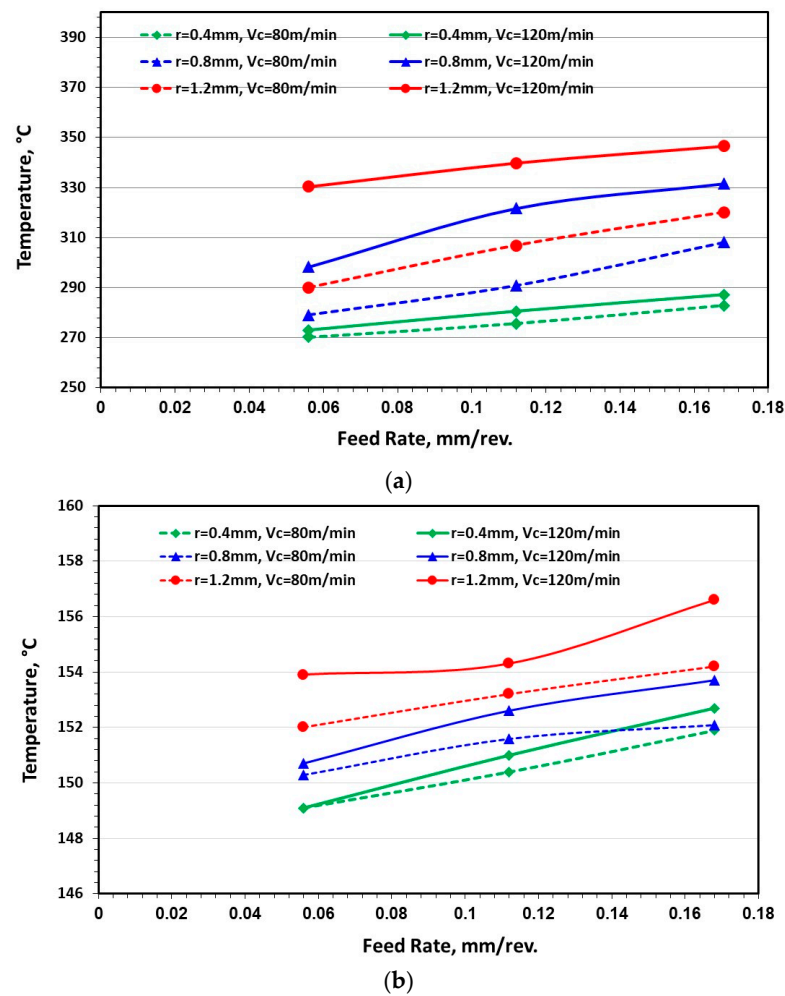
(**a**)

(**b**)

Figure 6. The relation between feed rate and cutting temperature at different tool nose radii and cutting speeds in (**a**) dry condition and (**b**) wet condition.

Table 5. Average percentage increase in temperature due to change in feed rate.

Nose Radius "*r*", mm	Feed Rate, "*FR*", mm/rev.	Temperature, "*T*" °C, at:	
		80 m/min	**120 m/min**
0.4	0.056	270.3	273.1
	0.112	275.7	280.6
	0.168	282.8	287.0
	$T_{avg.}$ %	4.6	5.0
0.8	0.056	279.1	298.3
	0.112	290.9	321.7
	0.168	308.2	331.6
	$T_{avg.}$ %	10.4	11.1
1.2	0.056	290.2	330.4
	0.112	306.9	339.8
	0.168	320.1	346.5
	$T_{avg.}$ %	10.3	4.8

Furthermore, Table 6 presents the $T_{avg.}$ % due to the change in "V_c". The influence of increasing "V_c" on the $T_{avg.}$ % was minimal, giving an average value of 1.36% with (r = 0.4 mm), 8.26% with (r = 0.8 mm), and 10.9% with (r = 1.2 mm). Briefly, the influence of increasing "V_c" on "$T_{avg.}$" is limited at small "r" and increases when increasing it.

Table 6. Average percentage increase in cutting temperature due to change in cutting speed.

Nose Radius "r", mm	Feed Rate, "FR", mm/rev.	Cutting Temperature, "T" °C, at:		Percentage Increase in Temperature, %	$T_{avg.}$ %
		80 m/min	**120 m/min**		
0.4	0.056	270.3	273.1	1.0	1.36
	0.112	275.7	280.6	1.7	
	0.168	282.8	287.0	1.4	
0.8	0.056	279.1	298.3	6.8	8.26
	0.112	290.9	321.7	10.5	
	0.168	308.2	331.6	7.5	
1.2	0.056	290.2	330.4	13.8	10.9
	0.112	306.9	339.8	10.7	
	0.168	320.1	346.5	8.2	

The effect of varying "r" solely on heating the cutting zone in the dry condition can be deduced from Table 7, where increasing "r" at constant "V_c" of 80 m/min increases the "T" by 7.3% at fixed "FR" (0.056 mm/rev.), 11.3% at fixed "FR" (0.112 mm/rev.), and 13.1% at fixed "FR" (0.165 mm/rev.). At higher "V_c" of 120 m/min, increasing "r" gives mostly a consistent increase in temperature of about 21% independent of "FR". Thus, the contribution of increasing "r" in heating at a high speed of 120 m/min is double that at a lower speed of 80 m/min.

Table 7. Average percentage increase in temperature due to change in nose radius.

Feed rate "FR", mm/rev.	Nose Radius "r", mm	Temperature °C at:	
		80 m/min	**120 m/min**
0.056	0.4	270.3	273.1
	0.8	279.1	298.3
	0.12	290.2	330.4
$T_{avg.}$ %		7.3	20.9
0.112	0.4	275.7	280.6
	0.8	290.9	321.7
	0.12	306.9	339.8
$T_{avg.}$ %		11.3	21.0
0.168	0.4	282.8	287.0
	0.8	308.2	331.6
	0.12	320.1	346.5
$T_{avg.}$ %		13.1	20.7

3.3. Effect of Feed Rate, Cutting Speed, and Nose Radius on Average Surface Roughness

Generally, surface roughness "R_a" was measured three times after each turning run, where average results were calculated, giving average surface roughness "Ra_{avg}". An example of actual surface morphology taken by optical microscope and its corresponding surface roughness profile pictured from the surface roughness tester is shown in Figure 7a,b, respectively. The cutting parameters of this example were "FR" = 0.056 mm/rev., V_c = 80 m/min, r = 0.4 mm, and DOC = 0.5 mm in the dry condition.
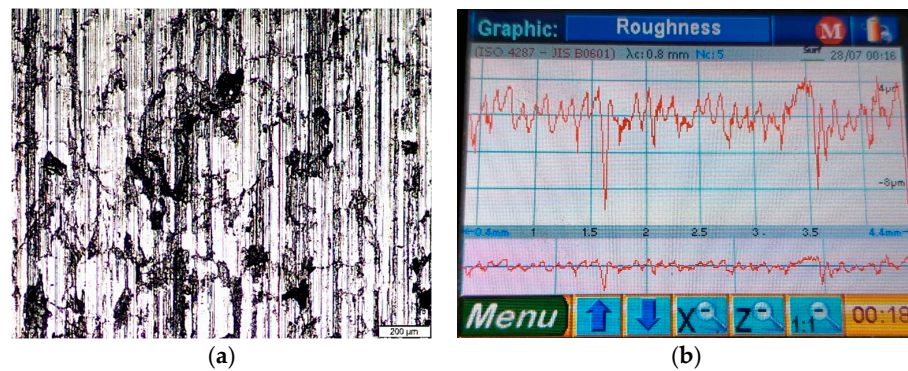
Figure 7. Surface roughness of grey iron after turning at "*FR*" = 0.056 mm/rev., *Vc* = 80 m/min, *r* = 0.4 mm, and *DOC* = 0.5 mm in the dry condition. (**a**) Optical microscope image; (**b**) screenshot of the corresponding surface roughness profile.

Figure 8a,b show the effect of increasing "*FR*" on the average surface roughness "Ra_{avg}" in the dry and wet conditions, respectively. Increasing "*FR*" increases the "$Ra_{avg.}$" in both the dry and wet conditions which are due to the increased advancing step/feed mark of the cutting edge per revolution as per İnce and Asiltürk [19], Gokkaya and Nalbant [20]. Figure 8a,b also shows the effect of varying "V_c" and "*r*" on "$Ra_{avg.}$". At constant "*FR*", lower "$Ra_{avg.}$" (i.e., better surface finish) is achieved at higher "V_c" compared to the lower one, which is probably due to the higher process stability accompanying higher speeds as found by Bhushan [21]. Furthermore, bigger "*r*" reduces "$Ra_{avg.}$" compared to smaller ones because smaller "*r*" yields a sharper feed mark on the workpiece surface (i.e., splintering effect) than bigger ones [19,20].

It can be inferred from the above results that "*FR*", "V_c", and "*r*" affect the "$Ra_{avg.}$", thus it might be interesting for the industry to evaluate the extent of influence of each parameter on it via simple calculations (i.e., the cutting parameter mostly affecting "$Ra_{avg.}$"). Table 8a,b presents the percentage increase in "Ra_{avg}" at constant "V_c" 80 and 120 m/min, respectively, in dry cutting. In both tables, the column titled "*Increase in surface roughness, %*" presents the incremental percentage increase in "Ra_{avg}" when increasing "*FR*", whereas the column titled "*Overall increase in "Ra_{avg}", %*" presents the difference between the highest and lowest "*FR*" at fixed "*r*". Comparing Table 8a,b shows that all values of "Ra_{avg}" corresponding to V_c = 80 m/min are higher than that obtained at V_c = 120 m/min due to a more stable process. Increasing "*FR*" by 200% increases the "Ra_{avg}" within 67–79% at V_c = 80 m/min, whereas "Ra_{avg}" is further increased at 120 m/min within 96–120%. This indicates that the increase in "Ra_{avg}" is more sensitive to the increase in "*FR*" at higher speeds than with lower ones.
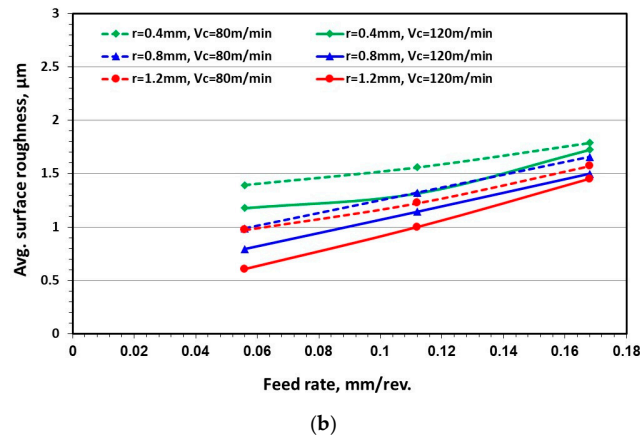

(**a**)

Figure 8. *Cont.*

(**b**)
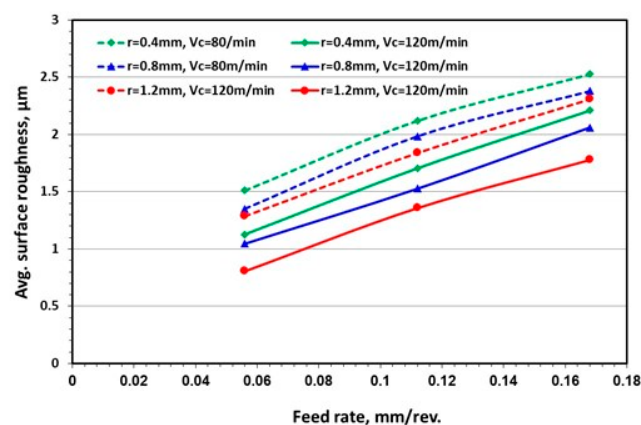
Figure 8. The relation between feed rate and average surface roughness at different tool nose radii and cutting speeds in (**a**) dry condition and (**b**) wet condition.

Table 9 shows the influence of increasing "V_c" on "Ra_{avg}" at constant "FR" and "r". Increasing "V_c" reduces "Ra_{avg}" (i.e., improves surface quality) in which the percentage reduction in "Ra_{avg}" increases when reducing "FR" as well as increasing "r". In general, the surface quality improvement ranged between 13–26% at "r" of 0.4 mm, 14–23% at 0.8 mm, and 23–38% at 1.2 mm, meaning that lower "FR" enhances surface finish by 26, 23, and 38% with nose radii of 0.4, 0.8, and 1.2 mm, respectively.

Table 8. Effect of feed rate in increasing average surface roughness at cutting speed (**a**) 80 m/min and (**b**) 120 m/min.

Nose Radius "r", mm	Feed Rate "FR", mm/rev.	"Ra_{avg}", μm	Increase in "Ra_{avg}", %	The Overall Increase in "Ra_{avg}", %
0.4	0.056	1.512		
			40	
	0.112	2.121		67
			19	
	0.168	2.528		
0.8	0.056	1.352		
			47	
	0.112	1.986		76
			20	
	0.168	2.381		
1.2	0.056	1.291		
			42	
	0.112	1.841		79
			25	
	0.168	2.311		

(**a**)

Table 8. *Cont.*

Nose Radius "r", mm	Feed Rate "FR", mm/rev.	"Ra_{avg}", μm	Increase in "Ra_{avg}" %	Overall Increase in "Ra_{avg}", %
0.4	0.056	1.126	51	96
	0.112	1.706	29	
	0.168	2.213		
0.8	0.056	1.048	45	96
	0.112	1.528	34	
	0.168	2.062		
1.2	0.056	0.808	68	120
	0.112	1.36	31	
	0.168	1.781		

(**b**)

Table 9. Effect of cutting speed in reducing average surface roughness.

Nose Radius "r", mm	Feed Rate "FR", mm/rev.	"Ra_{avg}", μm 80 m/min	"Ra_{avg}", μm 120 m/min	Percentage Reduction in "Ra_{avg}", %	Average Percentage Reduction in "Ra_{avg}", %
0.4	0.056	1.512	1.126	26	20
	0.112	2.121	1.706	20	
	0.168	2.528	2.213	13	
0.8	0.056	1.352	1.048	23	20
	0.112	1.986	1.528	23	
	0.168	2.381	2.062	14	
1.2	0.056	1.291	0.808	38	29
	0.112	1.841	1.36	26	
	0.168	2.311	1.781	23	

Similarly, Table 10 shows the influence of increasing "r" on "Ra_{avg}". Increasing "r" reduces "Ra_{avg}", where, at V_c = 80 m/min, increasing "r" improves surface finish by ≈12.1%, whereas at 120 m/min, the influence of "r" is 22.6%.

Therefore, based on the results presented in Tables 8–10, the cutting parameters that have the major influence of "$Ra_{avg.}$" are in the following order: "FR" with a value within 40~54%, while the "V_c" is within 20~29%, and "r" is within 12~22%. The aforementioned discussion was based upon simple calculations of results obtained directly from experiments; however, the next section deals with results that focus on creating inferences, which was carried out through full factorial design and ANOVA to study the combined effect of the studied machining parameters on the three responses.

Table 10. Effect of nose radius in reducing average surface roughness.

Feed Rate "FR", mm/rev.	Nose Radius "r", mm			Cutting Speed, "V_c" m/min.	Percentage Reduction in "Ra_{avg}", %	Average Percentage Reduction in "Ra_{avg}", %
	0.4	0.8	1.2			
0.056	1.512	1.352	1.291		14.6	
0.112	2.121	1.986	1.841	80 m/min	13.2	12.1
0.168	2.528	2.381	2.311		8.5	
0.056	1.126	1.048	0.808		19.5	
0.112	1.706	1.528	1.36	120 m/min	20.3	22.6
0.168	2.213	2.062	1.781		28.2	

3.4. Statistical Analysis

Table 11 summarizes ANOVA results for "Ra_{avg}.". The results show that three factors have a notable effect on "Ra_{avg}."; they are "FR", "V_c", and "r". The results also show that there is significant interaction between the coolant and the "FR". Examining the values of the adjusted sum of squares yields that the "FR" has the greatest effect on the "Ra_{avg}." variation, as shown earlier. Figure 9 illustrates the interaction plot between coolant and "FR" for "Ra_{avg}." where it can be seen that wet turning (i.e., coolant is on) at high "FR" reduces "Ra_{avg}.", whereas, at lower "FR", its effect is insignificant.

Table 11. ANOVA results for Ra_{avg}.

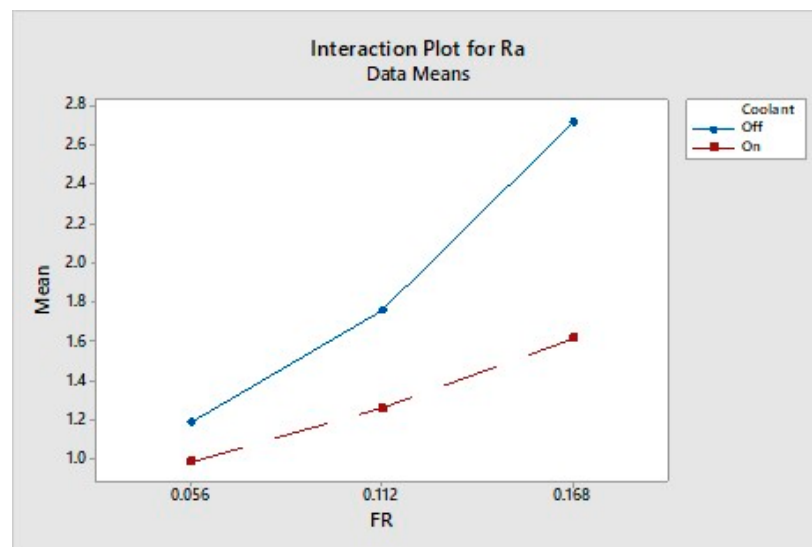| Source	DF	Adj SS	Adj MS	F-Value	*p*-Value
V_c	1	1.9895	1.9895	8.18	0.008
FR	1	6.9305	6.9305	28.50	0.000
Coolant	1	0.1150	0.1150	0.47	0.497
R	2	2.2202	1.1101	4.57	0.019
FR * Coolant	1	1.2083	1.2083	4.97	0.034
Error	29	7.0520	0.2432		
Total	35	22.6232			

Figure 9. Interaction plot for Ra_{avg}.

Table 12 shows the ANOVA output for the resultant force "R". The results show that the four studied factors have a significant effect on "R", and also, there is significant interaction between the coolant and the other three factors. Examining the values of the

adjusted sum of squares yields that "*FR*" has the greatest effect on "*R*". Figure 10 illustrates the significant interaction plots for "*R*" where wet turning (i.e., coolant is on) always reduces the "*R*" regardless of other factors settings. Figure 9a,c show that "*R*" decreases with increasing both "V_c" and "*r*", especially in dry turning (i.e., coolant off). Figure 9b shows that "*R*" also increases with increasing "*FR*", as reported earlier in Section 3.1.

Table 12. ANOVA results for "*R*".

Source	DF	Adj SS	Adj MS	F-Value	*p*-Value
V_c	1	252.25	252.25	70.42	0.000
FR	1	5018.49	5018.49	1401.05	0.000
Coolant	1	54.12	54.12	15.11	0.001
r	2	1928.52	964.26	269.20	0.000
V_c * Coolant	1	86.44	86.44	24.13	0.000
FR * Coolant	1	126.10	126.10	35.20	0.000
Coolant * *r*	2	118.78	59.39	16.58	0.000
Error	26	93.13	3.58		
Total	35	8136.09			

(**a**)

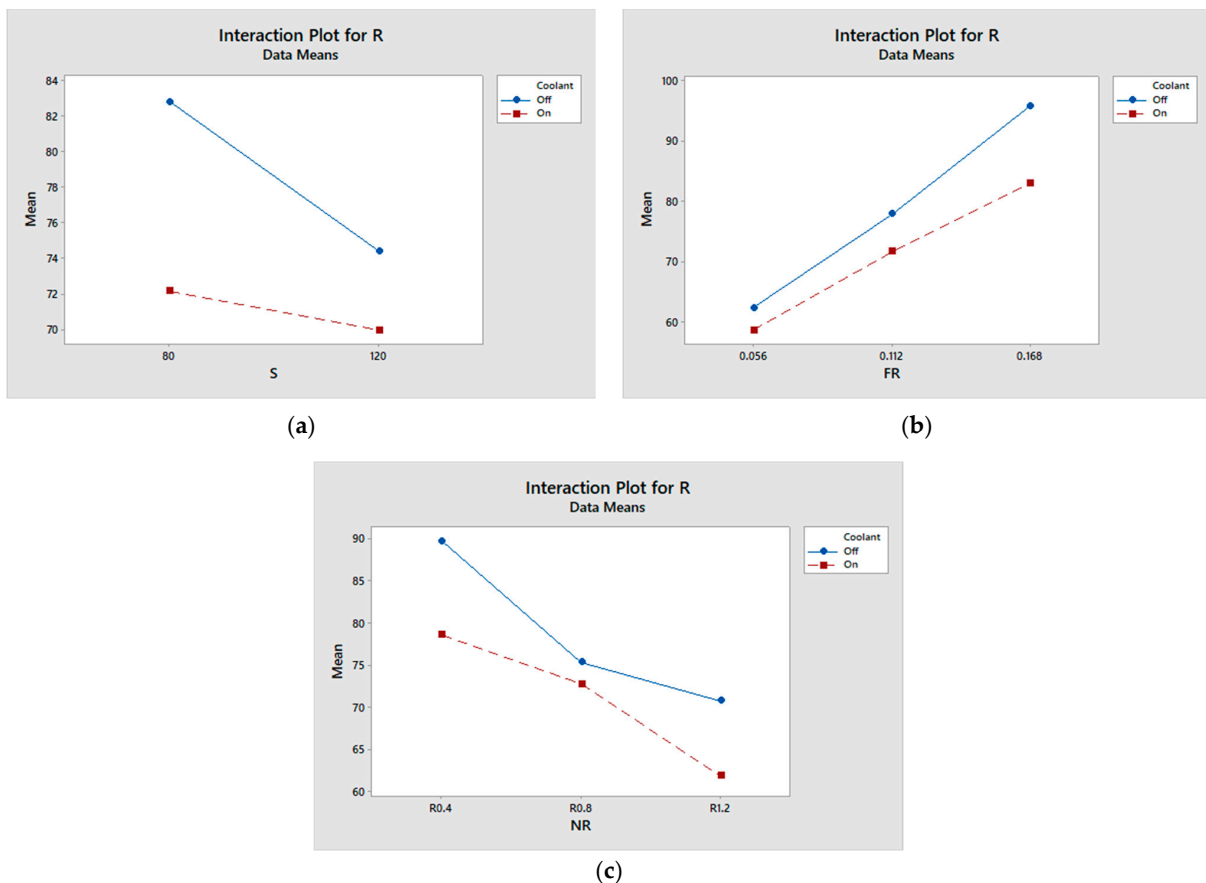(**b**)

(**c**)

Figure 10. Interaction plots for "R": (**a**) coolant vs. cutting speed, (**b**) coolant vs. feed rate, and (**c**) coolant vs. nose radius.

Table 13 summarizes ANOVA results for "*T*". The results show that only three studied factors have a significant effect on the "*T*"; they are the coolant, "V_c", and "*FR*". In addition, there is significant interaction between the coolant and the other three factors and also between the "V_c" and "*r*", all of which are in agreement with earlier results. Examining the

values of the adjusted sum of squares yields that the coolant and its interactions have the greatest effect on the temperature variation. Figure 11 illustrates the significant interaction plots for "*T*". Figure 11a–c show that wet turning (i.e., coolant on) always reduces the temperature regardless of other factors setting. It is also shown that the coolant effect on "*T*" is higher at high "V_c", feed rate, and nose radius. Figure 11d illustrates that the "*T*" decreases with the increase of nose radius. This phenomenon is more clear at high "V_c".
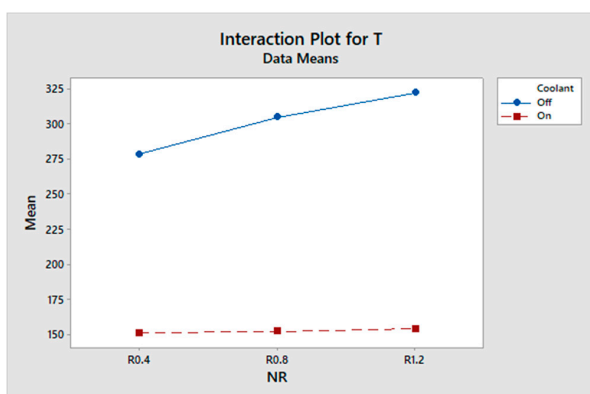
Table 13. ANOVA results for "*T*".

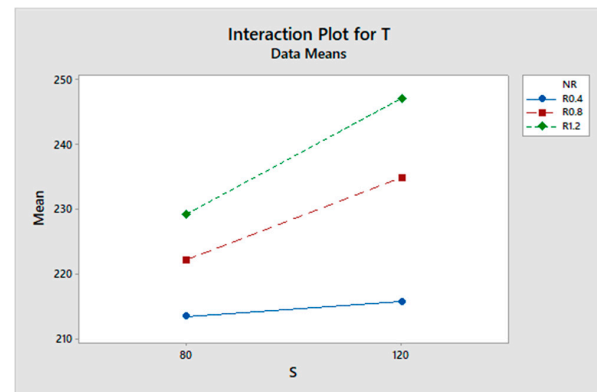| Source	DF	Adj SS	Adj MS	F-Value	*p*-Value
V_c	1	1077	1076.93	46.70	0.000
FR	1	978	977.93	42.41	0.000
Coolant	1	1897	1897.28	82.28	0.000
r	2	62	30.76	1.33	0.282
V_c * Coolant	1	834	834.25	36.18	0.000
Vc * *r*	2	379	189.38	8.21	0.002
FR * Coolant	1	570	570.37	24.74	0.000
Coolant * *r*	2	2574	1287.19	55.82	0.000
Error	24	553	23.06		
Total	35	212,204			
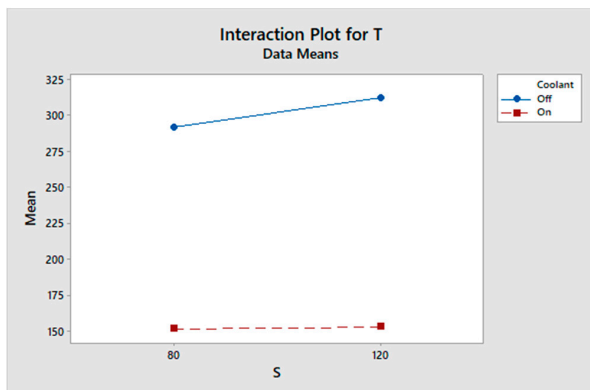
(**a**)
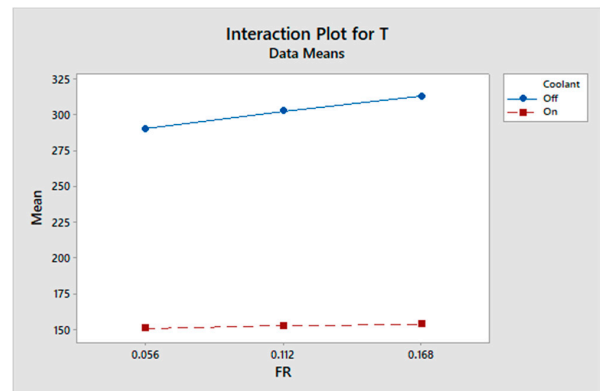
(**b**)

(**c**)

(**d**)

Figure 11. Interaction plots for T: (**a**) coolant vs. cutting speed, (**b**) coolant vs. feed rate, (**c**) coolant vs. nose radius, and (**d**) nose radius vs. speed.

The desirability function optimization tool in Minitab 18 was used to minimize "$Ra_{avg.}$", "R", and "T", and to maximize *MRR*. The priority was given to keep "$Ra_{avg.}$" below 0.8 μm (with a target of 0.7 μm), then to maximize *MRR* and minimize "T". The lowest priority was given to minimizing "R". Individual desirability (d) and composite desirability (D) has a range of 0.0 to 1.0. One denotes the ideal case, and zero illustrates the case when the response is outside its acceptable limits.

The optimum values for the factors were calculated to be "V_c" = 120 m/min, *FR* = 0.09 mm/rev, coolant on, and *r* = 1.2 mm. The expected optimum responses were calculated to be $Ra_{avg.}$ = 0.7 μm, *R* = 56 N, *T* = 157 °C, and *MRR* = 5466 mm³/min, as illustrated in Figure 12. For both "$Ra_{avg.}$" and "T", *DOC* is equal to 1.0, proving that these two responses will be optimized with perfection. For "R", *DOC* equals 0.9, showing it will be optimized to a good extent. For *MRR*, *DOC* = 0.4 because the feed rate had to be kept low to control the "$Ra_{avg.}$". The combined desirability, D, is equal to 0.79, proving that the combined optimization is well-achieved.
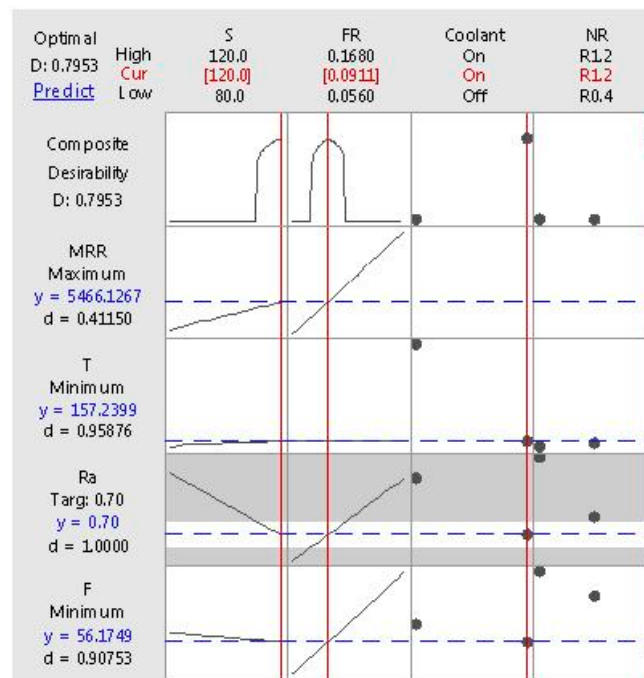

Figure 12. Optimization plot for responses using conventional cutting edge.

3.5. Validation and Verification of Optimum Conditions

The optimum conditions mentioned in Section 3.4 were verified by conducting three additional experiments, as presented in Table 14, which shows that the difference between the optimum values and the three validation values all lie within ± 5.5%, which is seen to be satisfactory.

Table 14. Validation and verification of optimum conditions.

Exp. #	Optimum Conditions			Validation			Percentage Difference, %		
	$Ra_{avg.}$, μm	"T" °C	"R" N	"$Ra_{avg.}$", μm	"T" °C	"R" N	$Ra_{avg.}$, μm	"T" °C	"R" N
1				0.74	162	55	5.7	3.1	−1.7
2	0.7	157	56	0.69	159	53	−1.5	1.2	−5.4
3				0.72	164	59	2.8	4.4	5.3

4. Conclusions

Based on the results reported, simple mathematical calculations and full factorial design, and ANOVA that were used to study the combined effect of the studied machining parameters on three responses, the following conclusions can be drawn from this work:

1　Increasing the feed rate increases the resultant force, cutting temperature, and surface roughness, whereas increasing cutting speed and nose radius increases the cutting temperature, which in turn reduces the resultant cutting force.

2　Increasing the feed rate increases cutting temperature by 5 to 11% depending on nose radius and cutting speed, whereas the influence of increasing cutting speed is limited at small nose radius and increases with it reaching about 11%.

3　Increasing nose radius increases cutting temperature depending mainly on cutting speed reaching a maximum of 21% at higher cutting speeds.

4　Considerably increasing the feed rate increases the average surface roughness to about 120% at high cutting speeds and a large nose radius. On the other hand, increasing cutting speed and nose radius reduce the surface roughness by a maximum of 29 and 23%, respectively.

5　Full factorial design and ANOVA showed that the coolant enhances the surface roughness, especially at higher cutting speeds.

6　Regarding the cutting force, the main effect comes from the feed rate. Turning the coolant on reduces the cutting force significantly.

7　Regarding the cutting temperature, the main contributor is the coolant, which is very much expected. The cooling affects the temperature more at high cutting speed, feed rate, and nose radius.

Author Contributions: Concept, M.M.E.R. and A.T.A.; methodology, M.M.E.R. and A.T.A.; software, A.A.A.-A. and F.B.; validation, A.A.A.-A., A.E and A.E.R.; formal analysis, M.M.E.R., A.E., A.E.R. and A.T.A.; investigation, A.E., A.E.R., A.A.A.-A. and F.B.; resources, M.M.E.R. and A.T.A.; data curation, M.M.E.R., A.T.A., A.E.R. and A.A.A.-A.; original draft preparation, M.M.E.R.; writing—review and editing, M.M.E.R., A.A.A.-A., F.B. and A.E.; visualization, F.B., A.E. and A.A.A.-A.; supervision, M.M.E.R. and A.T.A.; project administration, A.A.A.-A. and F.B.; funding acquisition, M.M.E.R. All authors have read and agreed to the published version of the manuscript.

Data Availability Statement: Not applicable.

Conflicts of Interest: The authors declare no conflict of interest.

References

1.　Chen, J.; Liu, W.; Deng, X. Tool life and wear mechanism of WC–5TiC–0.5VC–8Co cemented carbides inserts when machining HT250 grey cast iron. *Ceram. Int.* **2016**, *42*, 10037–10044. [CrossRef]

2.　Fischer, G.; Wei, Y.; Dontamsetti, S. Process-controlled machining of grey cast iron. *J. Mech. Work. Technol.* **1989**, *20*, 47–57. [CrossRef]

3.　Souza, J.V.C.; Nono, M.C.A.; Ribeiro, M.V. Cutting forces in turning of grey cast iron using silicon nitride-based cutting tool. *Mater. Des.* **2009**, *30*, 2715–2720. [CrossRef]

4.　Meng, F.; Zhang, Z.; Feng, J. A study investigating the cutting mechanism of compacted graphite iron based on a novel microstructure of finite element model. *J. Manuf. Process.* **2022**, *81*, 250–260. [CrossRef]

5.　Rajbongshi, S.K.; Borah, A.; Choudhury, P.K. Optimization of Process Parameters in Turning of Grey Cast Iron with Mixed Oxide Ceramic Tool using Taguchi's Approach. In Proceedings of the Conference on Design and Research (AIMTDR 2014), Guwahati, Assam, India, 12–14 December 2014.

6.　Korkmaz, M.E.; Günay, M. Finite Element Modelling of Cutting Forces and Power Consumption in Turning of AISI 420 Martensitic Stainless Steel. *Arab. J. Sci. Eng.* **2018**, *43*, 4863–4870. [CrossRef]

7.　Asiltürk, I.; Kuntoğlu, M.; Binali, R.; Akku, H.; Salur, E. A Comprehensive Analysis of Surface Roughness, Vibration and Acoustic Emissions Based on Machine Learning during Hard Turning of AISI 4140 Steel. *Metals* **2023**, *13*, 437. [CrossRef]

8.　Ogedengbe, T.S.; Yezeed, O.A.; Yussouf, A. Effect of annealing on machinability of grey cast iron. *J. Eng. Technol.* **2019**, *10*.

9. Binali, R.; Demirpolat, H.; Kuntoğlu, M.; Sağlam, H. Machinability Investigations Based on Tool Wear, Surface Roughness, Cutting Temperature, Chip Morphology and Material Removal Rate during Dry and MQL-Assisted Milling of Nimax Mold Steel. *Lubricants* **2023**, *11*, 101. [CrossRef]
10. Abbas, A.T.; El Rayes, M.M.; Al-Abduljabbar, A.A.; Ragab, A.E.; Benyahia, F.; Elkaseer, A. Effects of Tool Edge Geometry and Cutting Conditions on the Performance Indicators in Dry Turning AISI 1045 Steel. *Machines* **2023**, *11*, 397. [CrossRef]
11. Abbas, A.T.; Al-Abduljabbar, A.A.; El Rayes, M.M.; Benyahia, F.; Abdelgaliel, I.H.; Elkaseer, A. Multi-objective Optimization of Performance Indicators in Turning of AISI 1045 under Dry Cutting Conditions. *Metals* **2023**, *13*, 96. [CrossRef]
12. Adel, T.; Abbas, A.T.; Adham, E.; Ragab, A.; Benyahia, F.; Mahmoud, S.; Soliman, M.S. Taguchi Robust Design for Optimizing Surface Roughness of Turned AISI 1045 Steel Considering the Tool Nose Radius and Coolant as Noise Factors. *Adv. Mater. Sci. Eng.* **2018**, *2018*, 2560253. [CrossRef]
13. Kuntoğlu, M.; Sağlam, H. ANOVA and fuzzy rule-based evaluation and estimation of flank wear, temperature, and acoustic emission in turning. *CIRP J. Manuf. Sci. Technol.* **2021**, *35*, 589–603. [CrossRef]
14. Aouici, H.; Elbah, M.; Yallese, M.A. Performance comparison of the wiper and conventional ceramic inserts in hard turning of AISI 4140 steel: Analysis of machining forces and flank wear. *Int. J. Adv. Manuf. Technol.* **2016**, *87*, 2221–2244. [CrossRef]
15. Chen, Z.; Peng, R.L.; Zhou, J. Effect of machining parameters on cutting force and surface integrity when high-speed turning AD 730™ with PCBN tools. *Int. J. Adv. Manuf. Technol.* **2019**, *100*, 2601–2615. [CrossRef]
16. Thakur, D.G.; Ramamoorthy, B.; Vijayaraghavan, L. Machinability investigation of Inconel 718 in high-speed turning. *Int. J. Adv. Manuf. Technol.* **2019**, *45*, 421–429. [CrossRef]
17. Ali, M.H.; Ansari, M.N.M. The Effect of Nose Radius on Cutting Force and Temperature during Machining Titanium Alloy (Ti-6Al-4V). *Int. J. Mech. Mechatron. Eng.* **2014**, *8*, 2124–2127.
18. Bouchelaghem, H.; Yallese, M.A.; Amirat, A.T. Experimental Investigation and Performance Analyses of CBN Insert in Hard Turing of Cold Work Tool Steel (D3). *Mach. Sci. Technol.* **2010**, *14*, 471–501. [CrossRef]
19. İnce, M.A.; Asiltürk, İ. Effects of Cutting Tool Parameters on Surface Roughness. *Int. J. Eng. Sci.* **2015**, *4*, 15–22.
20. Gokkaya, H.; Nalbant, M. The effects of cutting tool geometry and processing parameters on the surface roughness of AISI 1030 steel. *Mater. Des.* **2007**, *28*, 717–721. [CrossRef]
21. Bhushan, R.K. Impact of nose radius and machining parameters on surface roughness, tool wear and tool life during turning of AA7075/SiC composites for green Manufacturing. *Bhushan Mech. Adv. Mater.* **2020**, *6*, 1. [CrossRef]